Molecular Systems Biology 6; Article number 394; doi:10.1038/msb.2010.51
Citation: ***Molecular Systems Biology*** **6:394**

www.molecularsystemsbiology.com

molecular systems biology

A diffusion-based neurite length-sensing mechanism involved in neuronal symmetry breaking

Michinori Toriyama[1], Yuichi Sakumura[2,3,*], Tadayuki Shimada[1], Shin Ishii[2,3,4,5] and Naoyuki Inagaki[1,3,*]

[1] Graduate School of Biological Sciences, Nara Institute of Science and Technology, Ikoma, Japan, [2] Graduate School of Information Science, Nara Institute of Science and Technology, Ikoma, Japan, [3] Institute for Bioinformatics Research and Development, Japan Science and Technology Agency (JST), Tokyo, Japan, [4] Graduate School of Informatics, Kyoto University, Uji, Japan and [5] Computational Science Research Program, RIKEN, Saitama, Japan

* Corresponding authors. N Inagaki, Graduate School of Biological Sciences, Nara Institute of Science and Technology, Ikoma, Nara 630-0192, Japan. Tel.: +81 743 72 5466; Fax: +81 743 72 5509; E-mail: ninagaki@bs.naist.jp or Y Sakumura, Graduate School of Information Science, Nara Institute of Science and Technology, Ikoma, Nara 630-0192, Japan. Tel.: +81 743 72 5467; Fax: +81 743 72 5509; E-mail: saku@is.naist.jp

Received 25.1.10; accepted 1.6.10

Although there has been significant progress in understanding the molecular signals that change cell morphology, mechanisms that cells use to monitor their size and length to regulate their morphology remain elusive. Previous studies suggest that polarizing cultured hippocampal neurons can sense neurite length, identify the longest neurite, and induce its subsequent outgrowth for axonogenesis. We observed that shootin1, a key regulator of axon outgrowth and neuronal polarization, accumulates in neurite tips in a neurite length-dependent manner; here, the property of cell length is translated into shootin1 signals. Quantitative live cell imaging combined with modeling analyses revealed that intraneuritic anterograde transport and retrograde diffusion of shootin1 account for its neurite length-dependent accumulation. Our quantitative model further explains that the length-dependent shootin1 accumulation, together with shootin1-dependent neurite outgrowth, constitutes a positive feedback loop that amplifies stochastic fluctuations of shootin1 signals, thereby generating an asymmetric signal for axon specification and neuronal symmetry breaking.
Molecular Systems Biology **6**: 394; published online 27 July 2010; doi:10.1038/msb.2010.51
Subject Categories: development; neuroscience
Keywords: feedback loop; neuronal polarity; quantitative modeling; shootin1; stochasticity

Introduction

Cell morphology and size must be properly controlled to ensure cellular function, and there has been significant progress in understanding the molecular signals that change cell morphology. However, the manner in which cells monitor their size and length to regulate their morphology is poorly understood (Dolznig *et al*, 2004; Marshall, 2004; Neumann and Nurse, 2007). Rat hippocampal neurons polarize in symmetrical *in vitro* environments (Craig and Banker, 1994; Arimura and Kaibuchi, 2005). These neurons first form several immature neurites (minor processes) that are similar in length, and at this stage the neurons appear symmetric (stage 2). Thereafter, one of these neurites outgrows its siblings to break this neuronal symmetry (stage 3). The longest neurite acquires axonal characteristics, whereas the others later become dendrites, to establish neuronal polarity. Thus, this break in symmetry is the initial step of neuronal polarization. The symmetry-breaking step reproduces even when the axon is transected at stage 3 (Goslin and Banker, 1989). After the transection, the longest neurite usually grows rapidly to become an axon, regardless of whether it is an axonal stump or an immature neurite. Elongation of an immature neurite of stage-2 neurons by mechanical tension also leads to its axonal specification (Lamoureux *et al*, 2002). These observations suggest that cultured hippocampal neurons can sense neurite length, identify the longest one, and induce its subsequent elongation for axonogenesis (Goslin and Banker, 1989). However, little is known about the mechanism for this process.

In relation to this question, intracellular signals that locally accumulate in a single neurite are reported to specify axons (Arimura and Kaibuchi, 2005; Jiang and Rao, 2005). Recent studies using live cell imaging revealed the remarkable dynamics of two such proteins, the kinesin-1 motor domain ($Kif5C^{560}$) and shootin1 (Jacobson *et al*, 2006; Toriyama *et al*, 2006). During the symmetry-breaking step, these molecules undergo a stochastic accumulation in multiple growth cones at the neurite tips, and eventually accumulate predominantly in a single neurite that subsequently grows to become an axon. As the accumulation of shootin1 in the growth cones

promotes neurite outgrowth (Shimada *et al*, 2008) and its RNAi-mediated knockdown inhibits neuronal polarization (Toriyama *et al*, 2006), asymmetric accumulation of shootin1 in a single neurite probably has a key role in axon specification and neuronal symmetry breaking. However, the manner in which the asymmetric signals of shootin1 and other polarity-related proteins originate during polarization is unknown.

In this study, we addressed these two questions: the mechanisms of neurite length sensing and the generation of asymmetric signals for neuronal symmetry breaking. We first demonstrated that shootin1 accumulated in growth cones in a neurite length-dependent manner. Thus, neurite length does affect a molecular signal, namely, shootin1 concentration. Quantitative live cell imaging of shootin1 dynamics combined with mathematical analyses revealed that its active anterograde transport and retrograde diffusion account for the neurite length-dependent accumulation of shootin1. We further quantified shootin1 upregulation and shootin1-induced neurite outgrowth, and integrated these data together with the quantitative dynamics of the neurite length-dependent shootin1 accumulation into a model neuron. The model neuron accumulated shootin1 predominantly in a single neurite, leading to its spontaneous breaking of symmetry. These data suggest that the present diffusion-based neurite length-sensing system, together with shootin1 upregulation and shootin1-induced neurite outgrowth, constitutes a core mechanism for the induction of neuronal symmetry breaking.

Results

Shootin1 accumulates predominantly in a neurite before neuronal symmetry breaking

We first examined the spatio-temporal dynamics of shootin1 accumulation during the symmetry-breaking step, by monitoring the fluorescence images of EGFP–shootin1 and the volume marker monomeric red fluorescent protein (mRFP) expressed in hippocampal neurons. Before symmetry breaking, the relative concentration of shootin1 (EGFP–shootin1/mRFP) underwent stochastic fluctuation in multiple growth cones at neurite tips (Figure 1A), as reported previously (Toriyama *et al*, 2006). Eventually, one of the neurites predominantly accumulated shootin1 and underwent a rapid outgrowth to break the neuronal symmetry. In all cases (n=10), neurons predominantly accumulated shootin1 in the nascent axon and in the established axon. A statistical analysis revealed that shootin1 concentration rose significantly in the nascent axon 10 min before its outgrowth spurt to break symmetry (n=10; P<0.03; compared with minor processes; arrows, Figure 1B).

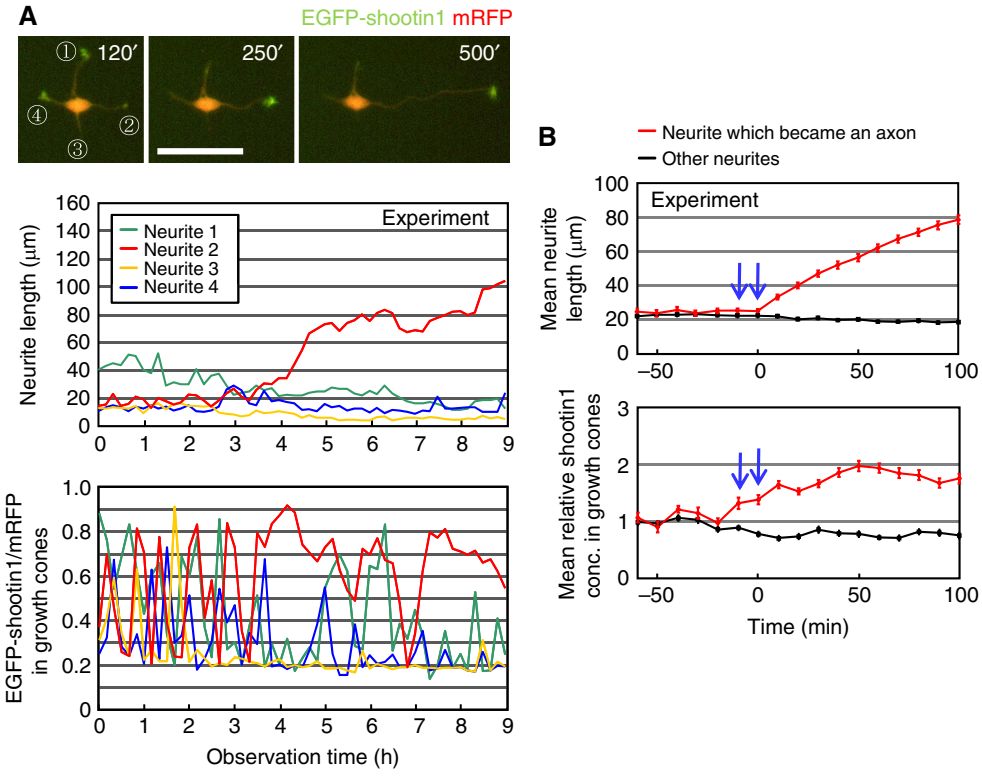

Figure 1 Asymmetric accumulation of shootin1 as an initial event in neuronal symmetry breaking. (**A**) A hippocampal neuron expressing EGFP–shootin1 (green) and mRFP (red) was observed under a time-lapse fluorescence microscope every 10 min. Neurite length and the relative shootin1 concentration (EGFP–shootin1/mRFP) in growth cones are plotted below the micrographs. (**B**) Statistical analysis of shootin1 accumulation during neuronal symmetry breaking. The top and bottom panels show the time courses for mean neurite length and mean relative shootin1 concentration in growth cones, respectively. The shootin1 concentration is shown as the multiple of the mean concentration in minor processes (means ± s.e., n=10, 0 min P<0.002, −10 min P<0.03; compared with minor processes, arrows). Red lines indicate the neurite that became an axon, whereas black lines indicate the mean values for the other neurites. Numbers in pictures of (A) are min. Bar, 50 μm. Source data is available for this figure at (www.nature.com/msb).

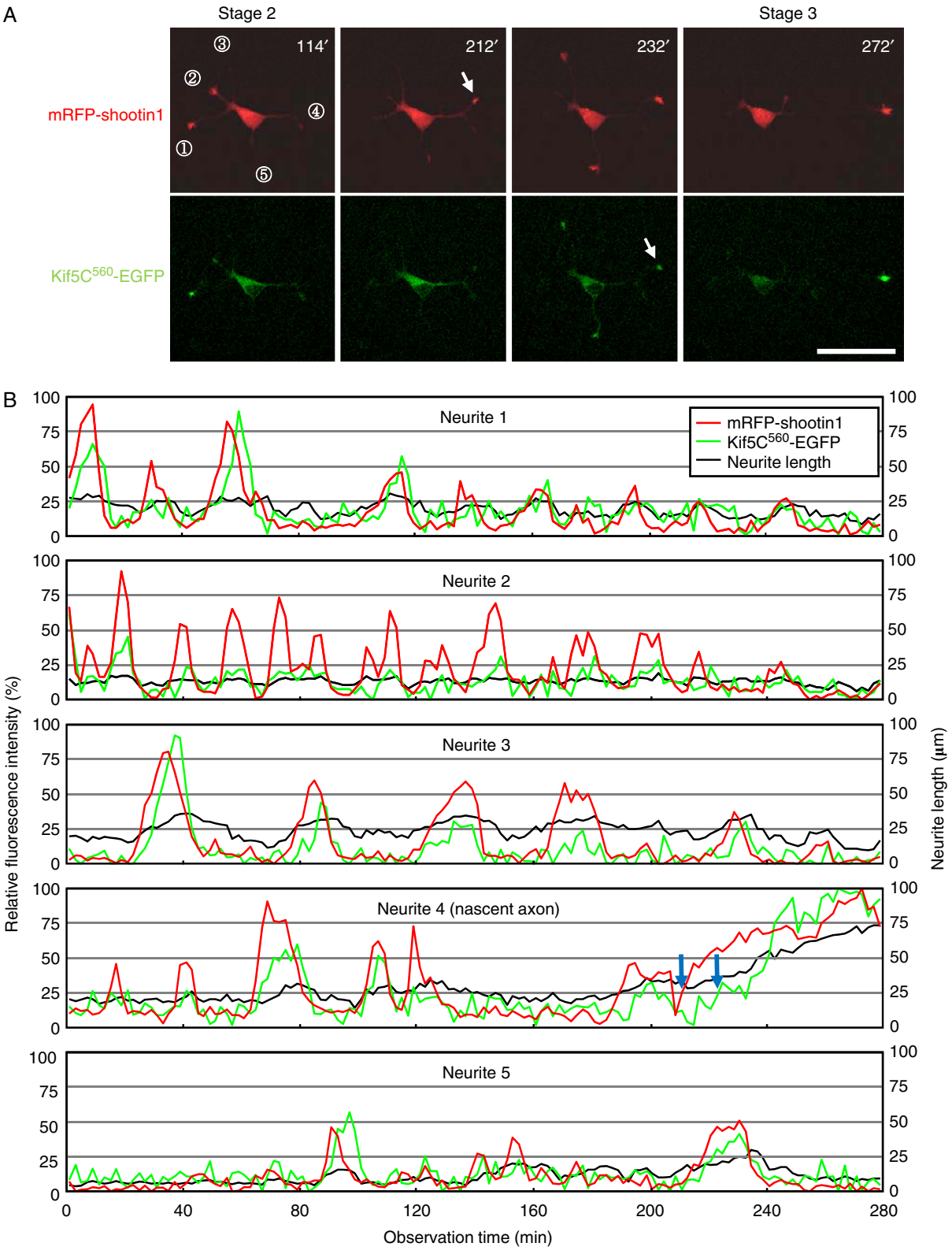

Figure 2 Accumulation of mRFP–shootin1 and Kif5C^{560}–EGFP during neuronal symmetry breaking. (**A**) A hippocampal neuron expressing mRFP–shootin1 (red) and Kif5C^{560}–EGFP (green) was observed under a time-lapse fluorescence microscope. (**B**) Relative fluorescence intensities of mRFP–shootin1 and Kif5C^{560}–EGFP in growth cones, expressed as the percentages of the maximal intensities observed in the nascent axon, and the neurite length of the neuron in (A) are plotted. The accumulations of shootin1 and Kif5C^{560} were compared at the time points when the relative intensities reached 25% (blue arrows), 50%, and 75% of their maximal values. Shootin1 accumulated significantly earlier than Kif5C^{560} at all time points. The time lags between the accumulations of the two molecules for these three relative values were 11.2 ± 3.2 (25%, $P<0.002$, $n=12$), 8.2 ± 1.6 (50%, $P<0.001$, $n=12$), and 9.5 ± 3.9 min (75%, $P<0.03$, $n=12$). Numbers in (A) are min. Bar, 50 μm. Source data is available for this figure at (www.nature.com/msb).

Recent time-lapse experiments reported that the predominant accumulation of Kif5C^{560} in a single neurite is one of the earliest markers of axonal specification (Jacobson *et al*, 2006). We therefore analyzed the accumulation of mRFP–shootin1 and Kif5C^{560}–EGFP in growth cones. Notably, these two molecules had a highly correlated accumulation in growth cones (Figure 2). In stage-2 neurons, mRFP–shootin1 and Kif5C^{560}–EGFP accumulated in the same neurite in many cases. During stage 2/3 transition, both molecules predominantly accumulated in the nascent axon and in the established axon. The accumulations of shootin1 and Kif5C^{560} were compared at the time points when the relative intensities reached 25 (blue arrows), 50, and 75% of their maximal intensities observed in the nascent axon. Shootin1 accumulated significantly earlier than Kif5C^{560} at all time points. The time lags between the accumulations of the two molecules for these three relative values were 11.2 ± 3.2 min (25%, $P<0.002$, $n=12$), 8.2 ± 1.6 min (50%, $P<0.001$, $n=12$), and 9.5 ± 3.9 min (75%, $P<0.03$, $n=12$). Taken together with our previous data, which show that the accumulation of shootin1 induces neurite outgrowth (Shimada *et al*, 2008) and that shootin1 RNAi inhibits neuronal polarization (Toriyama *et al*, 2006), these results underscore that the asymmetric accumulation of shootin1 is one of the critical events for neuronal symmetry breaking.

Shootin1 accumulates in growth cones in a neurite length-dependent manner

We previously reported that shootin1 is transported from the cell body to growth cones as discrete boluses with 'wave' structures through an actin- and myosin-dependent mechanism and diffuses back to the cell body (Toriyama *et al*, 2006). Wave is an actin-rich growth cone-like structure transported along the neurite shafts, and is thought to be involved in the anterograde transport of actin and actin-associated proteins (Ruthel and Banker, 1998, 1999; Flynn *et al*, 2009). It was proposed that such an anterogradely transported diffusible molecule might accumulate in growth cones in a neurite length-dependent manner (Goslin and Banker, 1989; Toriyama *et al*, 2006), because its retrograde diffusion possibly becomes slower as the neurites extend. To test this hypothesis, we next examined the relationship between the shootin1 concentration in growth cones and neurite length. We quantified shootin1 immunoreactivity and staining of a blue volume marker, CMAC (7-amino-4-chloromethylcoumarin), in growth cones of neurites of stage-2 and -3 neurons ($n=1743$). The relative concentration of shootin1 (shootin1 immunoreactivity/CMAC staining) varied considerably in individual growth cones (Figure 3A), influenced by the stochastic arrival of shootin1 boluses at the growth cones (see below, Figure 4). Nevertheless, a statistical analysis revealed a significant positive correlation between the shootin1 concentration in growth cones and neurite length (Figure 3A, Supplementary Table I).

To directly confirm the effect of neurite length on shootin1 accumulation in growth cones, we transected the axons of stage-3 neurons, in which shootin1 is predominantly concentrated, and examined its reaccumulation in growth cones by immunocytochemistry 6 h after transection. Two types of axonal transection were performed: (1) axonal stumps were >20 μm longer than the other neurites (long axonal stump, Figure 3C) and (2) axonal stumps were not longer than the other neurites (short axonal stump, Figure 3D; see Materials and methods section for detail). A total of 45 ± 4.4% ($n=3$, 93 neurons examined) of neurons with a long axonal stump reaccumulated shootin1 at the stump (Figure 3C and E). A significantly smaller number (13 ± 4.0%; $n=5$, 107 neurons examined) of neurons with short axonal stumps accumulated shootin1 at this site (Figure 3E). On the other hand, 17 ± 7.1% of neurons with long axonal stumps accumulated shootin1 in the other neurites, whereas a significantly larger number (59 ± 5.3%) of neurons with short axonal stumps accumulated shootin1 in the other neurites (Figure 3D and E). In neurons with short axonal stumps, we occasionally observed cells bearing a neurite >20 μm longer than the axonal stump ($n=20$; Figure 3F). The majority (65%) of such neurons accumulated shootin1 in the longest neurite, whereas 20 and 25% accumulated shootin1 in the axonal stump and in other neurites, respectively. These results indicate that shootin1 accumulates in growth cones in a neurite length-dependent manner, regardless of whether the neurites are axonal stumps or minor processes.

Anterograde transport and length-dependent retrograde diffusion account for neurite length-dependent shootin1 accumulation

We next examined whether the neurite length dependency of shootin1 accumulation can be explained by its anterograde transport and retrograde diffusion. Hodgkin and Huxley (1952b) demonstrated quantitatively that the action potential in a squid giant axon can be explained by the dynamics of potassium conductance and sodium conductance. To do so, they quantified the dynamics of potassium and sodium conductances, and fitted them into mathematical models. The parameters of the models were derived entirely from quantitative experimental data, without any adjustment. They then integrated both models, thereby showing good agreement between the reconstructed action potential and the experimentally observed action potential. Following this

Figure 3 Neurite length-dependent accumulation of shootin1. (**A**) Experimental data showing the relationship between neurite length and shootin1 accumulation in growth cones. Hippocampal neurons were double stained with an anti-shootin1 antibody and the volume marker CMAC (left). The relative shootin1 concentration (shootin1/CMAC) in growth cones is plotted against neurite length ($n=1743$, right). (**B**) Modeling data showing the relationship between neurite length and shootin1 accumulation in growth cones. Shootin1 accumulation was calculated by substituting the experimental data for neurite length in (A; $n=1743$) into Equation (3). The shootin1 concentration was sampled at $t=1000$ min for each calculation. Data of black spots with bars in (A) and (B) are means ± s.e. (C–F) Axons of stage-3 hippocampal neurons were transected (arrows, **C**, **D**, **F**). At 6 h after transection, neurons were fixed and stained with an anti-shootin1 antibody (right). Two types of axonal transection were performed: long axonal stump (C) and short axonal stump (D, F). For details, see Results section. The data in (**E**) represent the percentages of neurons that accumulated shootin1 in axonal stumps and in other neurites, and is shown as mean ± s.e. values (**$P<0.01$; $n=3$; a total of 200 neurons were examined). Bars: (A) 20 μm; (C, D, F) 50 μm. Source data is available for this figure at (www.nature.com/msb).

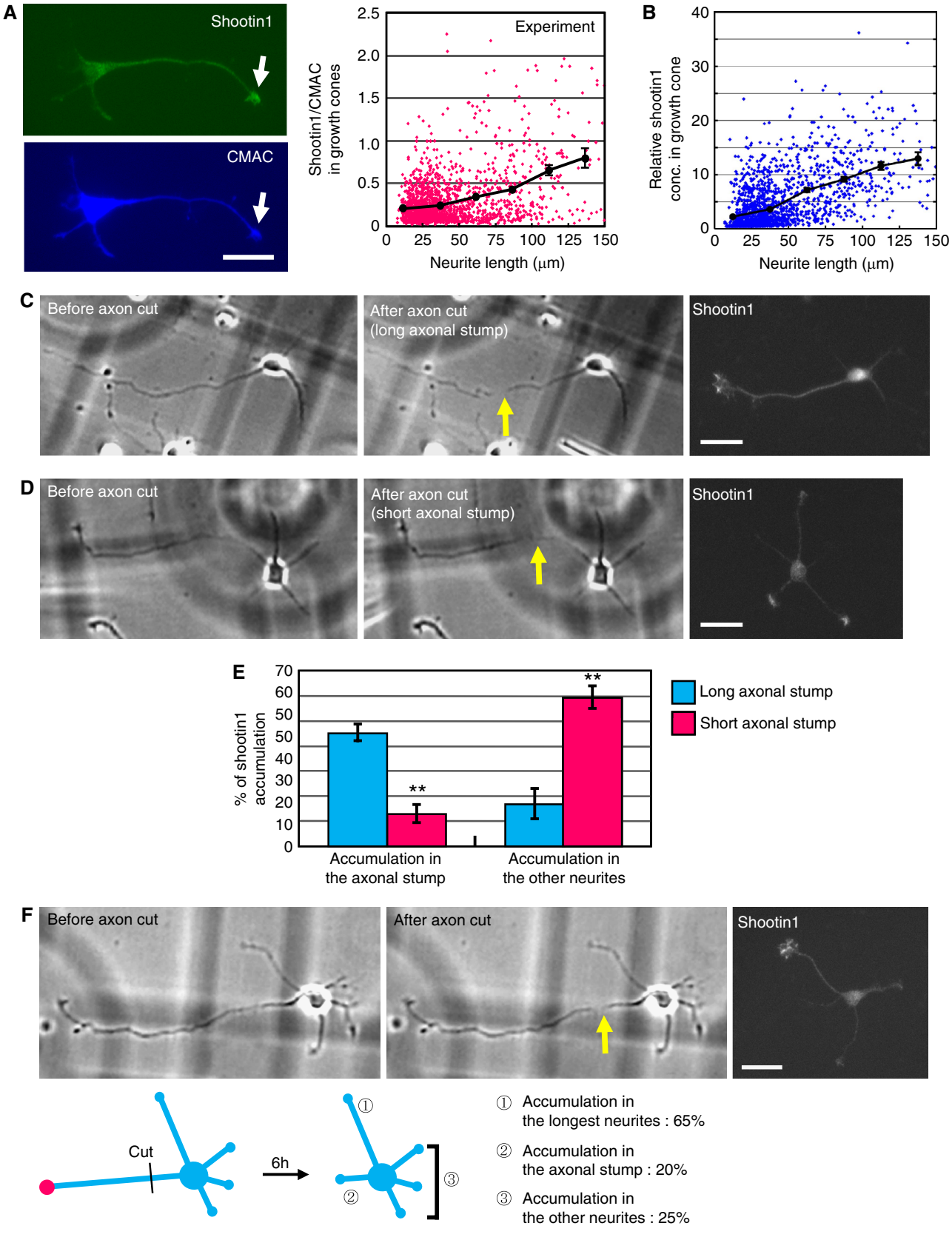

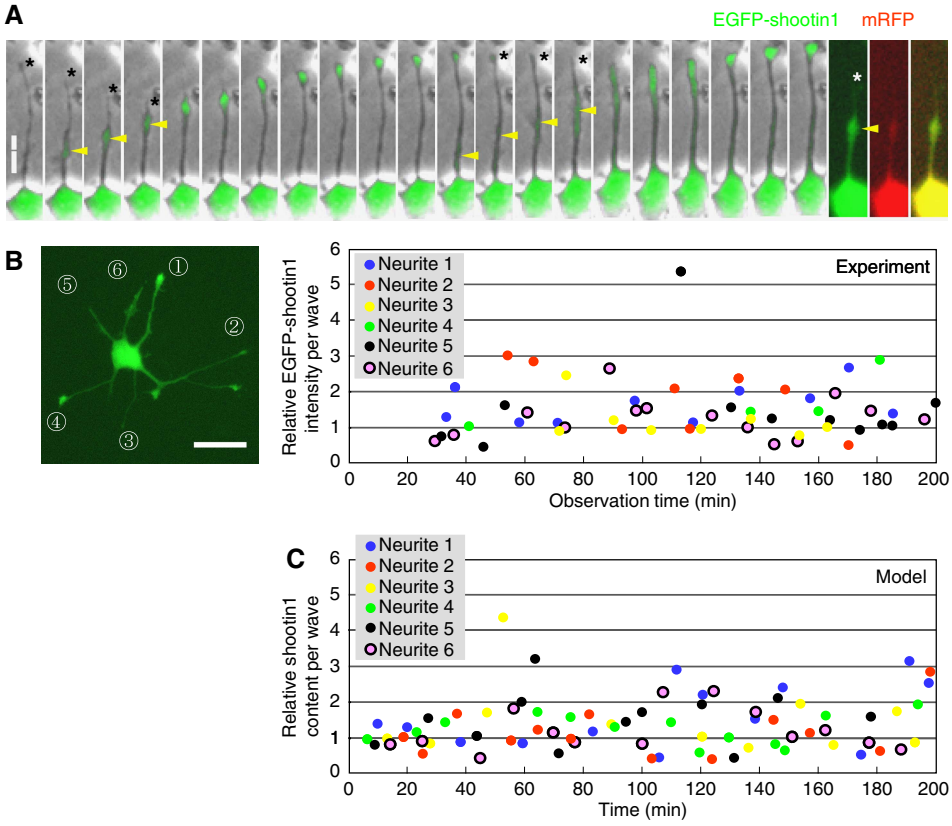

Figure 4 Stochastic anterograde transport of shootin1. (**A**) Stage 2 hippocampal neurons expressing EGFP–shootin1 (green) and the volume marker mRFP (red) were observed under a time-lapse fluorescence microscope every 2 min. Arrowheads indicate boluses of EGFP–shootin1 in waves, whereas asterisks denote a growth cone. (**B**) The left micrograph shows the six growth cones of the neuron in (A). The right graph shows the timings of wave arrival at growth cones 1–6 and the relative fluorescence intensities of EGFP–shootin1 in individual waves. (**C**) Timing of shootin1 arrival at six growth cones and the relative shootin1 content in individual waves determined from gamma distributions in Supplementary Figure 1A. Bars, 20 μm. Source data is available for this figure at (www.nature.com/msb).

strategy, we quantified the anterograde transport and retrograde movement of shootin1, fitted them to mathematical equations, and integrated them into a model.

Figure 4A shows the transport of EGFP–shootin1 from the cell body to a growth cone in a stage-2 neuron. Boluses enriched with EGFP–shootin1 (arrowheads) traveled along neurite shafts at an average rate of 4.7 ± 0.2 μm/min (n=24), and their arrival at growth cones (asterisks) increased the local concentrations of shootin1. The boluses contained variable amounts of EGFP–shootin1, and appeared repeatedly but irregularly in neurites at mean intervals of 17 min (n=55; Figure 4B). The coefficient of variation in the interval of their appearance was 0.86 (n=55), suggesting that shootin1 is transported in a stochastic manner. Together with the quantitative data of shootin1 and morphometry data of cultured neurons (Supplementary Figure 1), the active transport ($w(t)$) was modeled as the sum of temporally discrete events, each of which is modeled by the Gaussian function $g(t)$ (Supplementary Figure 1D),

$$w(t) = \frac{V_w}{V} w_{\mathrm{avg}} \sum_j a_j g(t - t_j) \qquad (1)$$

where V and V_w are volumes of the growth cone and wave, w_{avg} the average shootin1 concentration in the wave, and t the time. The stochasticities of the amplitude (a_j) and occurrence time (t_j) of the transport (red bars, Supplementary Figure 1A) were modeled by gamma distributions (blue curves). As shown in Figure 4C, Equation (1) described the stochastic transport of shootin1 (Figure 4B) with fair accuracy.

To quantify the retrograde movement of shootin1, photoconvertible Kaede–shootin1 expressed in growth cones was converted from green to red by UV light (arrows, Figure 5A), and its movement was monitored. To avoid the influence of the anterograde shootin1 transport, we monitored the movement only during the intermissions between apparent shootin1 transports. During these time-lapse observations, red Kaede–shootin1 in the growth cone gradually spread to the neurite shaft, cell body, and to other neurites (Figure 5A). If we assume that shootin1 diffuses passively in the neurite shaft, the differential equation of shootin1 concentration (C) in the growth cone can be expressed as

$$\frac{\mathrm{d}C}{\mathrm{d}t} = -\frac{AD}{VL}(C - C_0) \qquad (2)$$

where A is the cross-sectional area of the neurite, D the diffusion coefficient, L the neurite length, and C_0 the shootin1 concentration in the cell body. Equation (2) follows the well-established Fick's law (van Ooyen *et al*, 2001; Keener, 2002; see Materials and methods section and Supplementary information for detail). The amount of red Kaede–shootin1 in growth cones decayed exponentially, concurrent with its increase in

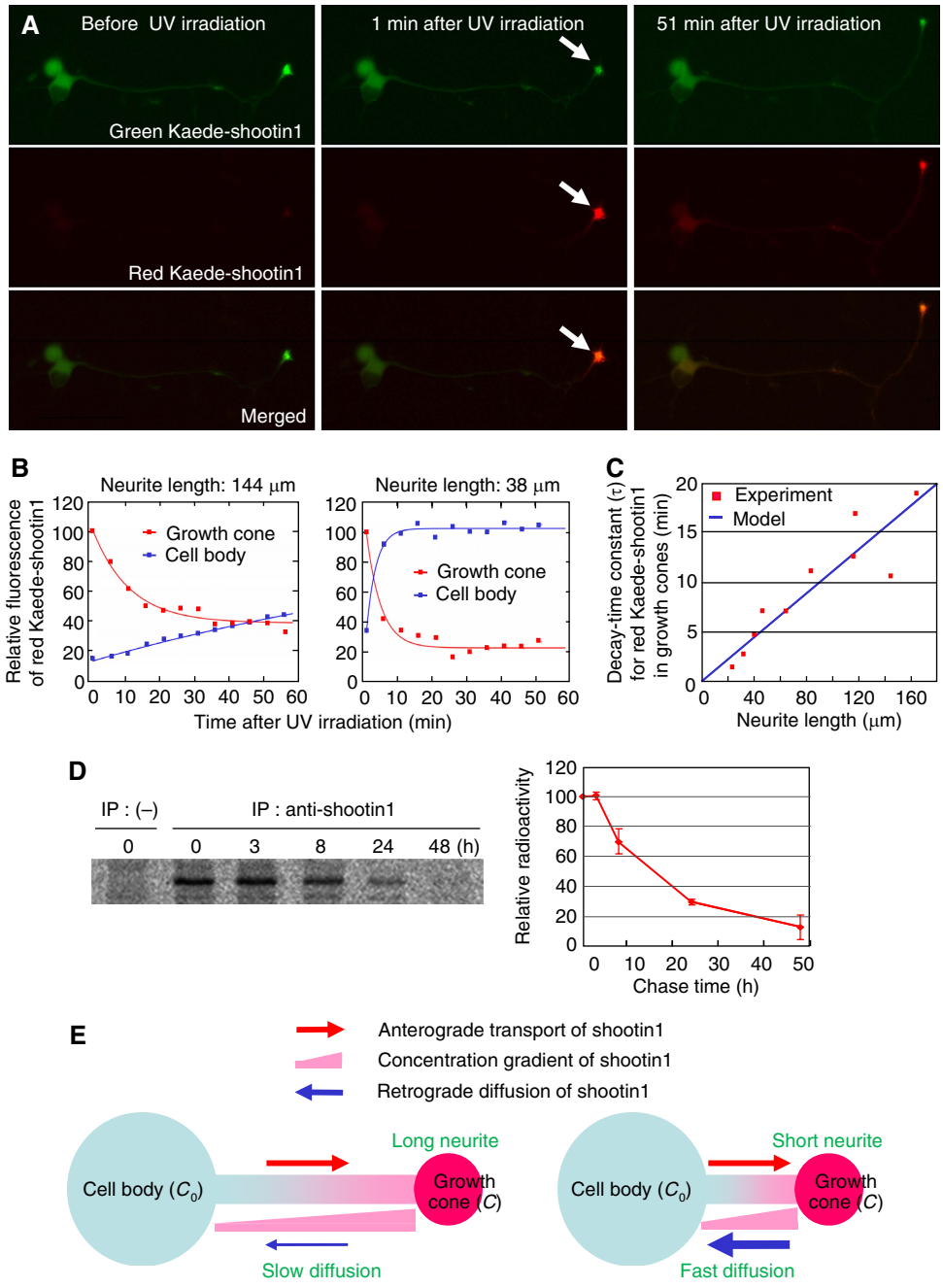

Figure 5 Neurite length-dependent retrograde diffusion of shootin1. (**A**, **B**) Kaede–shootin1 expressed in hippocampal neurons was converted from green to red using UV light at growth cones (A, arrows). The fluorescence of red Kaede–shootin1 in the growth cones and cell bodies was quantified under a time-lapse fluorescence microscope every 5 min (B). The fluorescence intensity was normalized by setting the intensity in the growth cones at time 0–100. (**C**) The relationship between neurite length and the decay-time constant (τ) of red Kaede–shootin1 in growth cones was plotted (red). (**D**) Cultured hippocampal neurons were labeled for 1 h with [^{35}S]methionine and [^{35}S]cysteine. The cells were then lysed after the indicated time, and immunoprecipitation was performed with or without anti-shootin1 antibody. Immunoprecipitated shootin1 resolved by SDS–PAGE was visualized by autoradiography. The graph shows percentage decrease in band intensity as mean ± s.e. (n=3). The pulse-chase analysis revealed that the turnover rate ($t_{1/2}$) of shootin1 in cultured hippocampal neurons was 17.8 h, which was much slower than the decay rate of red Kaede–shootin1 in growth cones in (B). Therefore, protein degradation does not significantly contribute to the delay in shootin1. (**E**) A model for diffusion-based neurite length-dependent shootin1 accumulation in growth cones. Bar, 50 μm. Source data is available for this figure at (www.nature.com/msb).

the cell body (Figure 5B). This is consistent with the equation $VC=ae^{-t/\tau}+b$, which is derived from the simultaneous differential equations for C and C_0 with constant parameters a, b, and τ (see Supplementary information). The decay rate was slower in the growth cones of longer neurites than in those of shorter neurites (Figure 5B), consistent with Equation (2). Furthermore, the decay time constant, τ, showed a linear relationship with neurite length L (n=10; Figure 5C), consistent with the formula $\tau=(VV_0L)/(AD(V+V_0))$, where V_0 is the volume of the cell body (see Supplementary information

for details). Thus, the dynamics of red Kaede–shootin1 follows the equations describing one-dimensional passive diffusion; we also confirmed that protein degradation and active retrograde transport does not significantly contribute to the dynamics of shootin1 in the growth cone (Figure 5D and Supplementary Figure 2). Using the experimental data in Figure 5B and C (n=10 neurites), parameters of Equation (2) were estimated using a least-squares method (Supplementary Table IID). As a result, Equation (2) (curves, Figure 5B) described the retrograde movement of shootin1 (dots, Figure 5B) fairly well.

To determine whether the neurite length-dependent shootin1 accumulation in the growth cone can be explained by the combination of anterograde transport (Equation (1)) and retrograde diffusion (Equation (2)), we combined Equations (1) and (2) as

$$\frac{dC}{dt} = -\frac{AD}{VL}(C - C_0) + w(t) \qquad (3)$$

As shown in Figure 3B and Supplementary Table I, the shootin1 accumulation in a growth cone, calculated using Equation (3), was neurite length dependent and showed excellent agreement with the experimental data (Figure 3A). Notably, the model also simulated the considerable variation among individual data. These results suggest that the neurite length-dependent accumulation of shootin1 is quantitatively explained by its anterograde transport and length-dependent passive diffusion, thereby providing a mechanistic basis for the length dependency of shootin1 accumulation (Figure 5E).

Integration of shootin1 upregulation, shootin1-induced neurite outgrowth, and neurite length-dependent shootin1 accumulation results in spontaneous neuronal symmetry breaking

The present length-dependent shootin1 accumulation in growth cones constitutes a local positive feedback interaction with the previously reported shootin1-induced neurite outgrowth (Shimada *et al*, 2008), and might contribute to neuronal symmetry breaking (Figure 6A). To test this hypothesis, we again adopted the strategy of Hodgkin and Huxley (1952b). We performed quantitative modeling of the shootin1-induced neurite outgrowth (Shimada *et al*, 2008) and shootin1 upregulation (Toriyama *et al*, 2006), and then integrated these models together with that of shootin1 accumulation in growth cones (Equation (3)) into a model neuron.

To model shootin1-induced neurite outgrowth, we introduced a simplified mathematical equation based on available mechanistic information. As shootin1 accumulation in growth cones produces a traction force ($f_s(C)$) for neurite outgrowth by interacting with actin filaments and L1-CAM (Shimada *et al*, 2008) and neurite length-dependent neurite tension ($f_l(L)$; Lamoureux *et al*, 1989) retract neurites, we assumed that shootin1-induced neurite outgrowth is regulated primarily by the balance between the two mechanical forces $f_s(C)$ and $f_l(L)$ (Figure 6B). In addition, we also considered that an increase in neurite length consumes intracellular material molecules required for the construction of the neurite shaft (Figure 6B). For simplicity of the model, we used tubulin, the most abundant protein in the neurite shaft (Van de Water and Olmsted, 1980; Gauss *et al*, 1999), as a representative of the material molecules that comprise the neurite shaft. The velocity of neurite outgrowth (dL/dt) was modeled with $f_s(C)$, $f_l(L)$, and the intracellular concentration of tubulin (M), by adopting the previously described force–velocity relationship derived from thermodynamics (Hill, 1987; Dogterom and Yurke, 1997) as follows,

$$\frac{dL}{dt} = \delta k_{on} M - \delta k_{off} \exp[-\kappa f_s(C) + \kappa f_l(L)] \qquad (4)$$

with a thermodynamic parameter κ. The constants δ, k_{on}, and k_{off} are the size of the material molecule, the rate constant of its insertion into the neurite shaft, and the rate constant of its deletion, respectively (Figure 6B). A detailed explanation of Equation (4) is described in Materials and methods section.

To determine the parameters of Equation (4), three stage-2 neurons expressing EGFP–shootin1 and mRFP were observed under a time-lapse microscope (Figure 4A), and the relative shootin1 concentration in the growth cones (EGFP–shootin1/mRFP) and neurite outgrowth velocity were quantified. We observed a strong positive correlation between the shootin1 concentration in the growth cone and the velocity of neurite outgrowth (Figure 6C and D). Using these data, parameters of Equation (4) were estimated for each of the three neurons 1–3 using a least-squares method. The obtained parameter sets were similar among the three neurons (Supplementary Table IIE). Despite the simplicity of the formulation, introduction of the parameter set derived from neuron 1 into Equation (4) described the quantitative correlation between shootin1 concentration in the growth cone and neurite outgrowth velocity with reasonable accuracy (Figure 6D). Similar data were obtained when the parameter set derived from neuron 2 or 3 was introduced into Equation (4) (data not shown). Although other types of equations might describe shootin1-induced neurite outgrowth equally well, we consider that Equation (4) provides an appropriate model for our purpose.

Shootin1 upregulation in cultured hippocampal neurons was quantified by immunoblot analysis (Figure 6E). The experimental data (red dots, Figure 6F) were fitted to a Hill-type formula,

$$S = V_0 \left\{ \frac{1.9}{1 + (t/3199)^{-2.5}} + 0.07 \right\} \qquad (5)$$

to quantitatively model shootin1 upregulation (red curve, Figure 6F). We also quantified the α-tubulin expression and fitted the data to a Hill-type formula (Figure 6E and F).

Integration of Equation (3–5) into the model neuron (Figure 7A, see Materials and methods section for detail) induced a stochastic accumulation of shootin1 in multiple growth cones (Figure 7B), as observed in cultured neurons (Figure 1A). One of the neurites then showed predominant shootin1 accumulation and rapid outgrowth, thereby breaking the neuronal symmetry. Symmetry breaking occurred in model neurons bearing different numbers of neurites, ranging from three to six (Figure 7B and Supplementary Figure 3). In addition, any parameter set derived from the three cultured neurons (Supplementary Table IIE) broke symmetry of the model neuron (data not shown), illustrating the robustness of symmetry breaking by our model. Statistical analyses showed

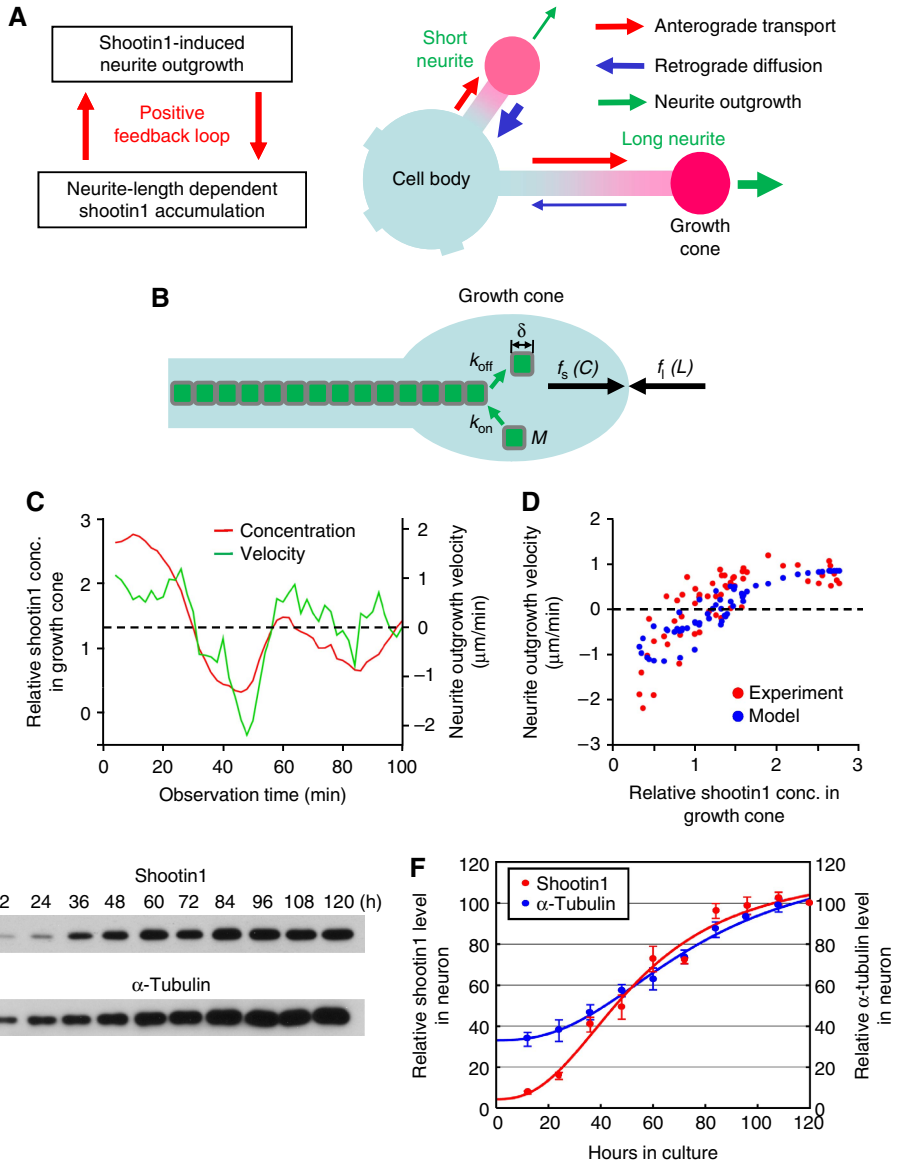

Figure 6 Modeling of shootin1-induced neurite outgrowth and shootin1 upregulation. (**A**) A model showing that a local positive feedback loop between the length-dependent shootin1 accumulation and shootin1-induced neurite outgrowth contributes to neuronal symmetry breaking. (**B**) We assumed that shootin1-induced neurite outgrowth is regulated primarily by the balance between the shootin1-induced traction force ($f_s(C)$) and neurite length-dependent neurite tension ($f_l(L)$), and secondarily by the intracellular concentration (M) of free material molecules required for the construction of the neurite shaft. (**C**) The relative shootin1 concentration in a growth cone (EGFP–shootin1/mRFP) and the corresponding neurite outgrowth velocity of a neurite in Figure 4B. (**D**) Phase plot of the relative shootin1 concentration in the growth cone and the corresponding neurite outgrowth velocity. Red points were plotted from the experimental data in (C), whereas the velocities represented by blue points were calculated by substituting the values for shootin1 concentration and neurite length in (C) into Equation (4). (**E**, **F**) Proteins from 1.7×10^5 neurons and 1.7×10^4 neurons were analyzed with anti-shootin1 and anti-α-tubulin antibodies, respectively (E). The band densities of shootin1 and α-tubulin were measured using a densitometer (F). The relative levels of shootin1 and α-tubulin were rescaled by normalizing the values at 120 h in culture to 100 (mean ± s.e., n=3). The curves were fitted to the experimental values using a Hill-type formula. Source data is available for this figure at (www.nature.com/msb).

that the time courses of shootin1 accumulation and symmetry breaking are similar between the model and cultured neurons (Figures 1B and 7C). The shootin1 concentration in the model rose significantly in the nascent axon 10 min before its outgrowth spurt to break symmetry (arrows, n=100, $P<0.001$; compared with minor processes), as was observed in cultured neurons. Interestingly, the generation of continuous anterograde transport of shootin1 in our model neuron impaired the symmetry-breaking process (Figure 7D).

In addition to these typical symmetry-breaking processes, previous studies have reported atypical behaviors of cultured neurons. During polarization, some hippocampal neurons replace the axon-like outgrowth of one neurite with another, which subsequently becomes an axon (Dotti *et al*, 1988). This atypical symmetry breaking was also observed in the model (Supplementary Figure 4A). A minor population of cultured neurons (2.5–5%) forms multiple axons (Jiang *et al*, 2005; Toriyama *et al*, 2006; Mori *et al*, 2007). We also noted the

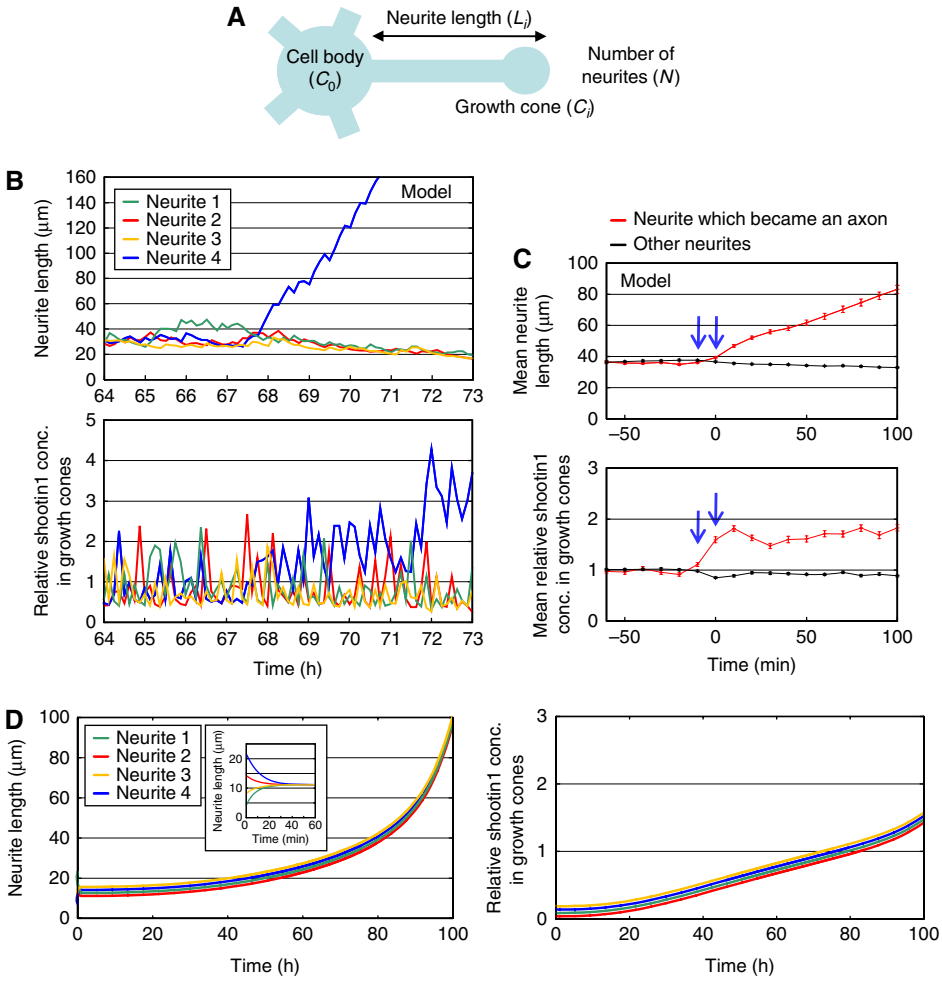

Figure 7 Symmetry breaking of the model neuron. (**A**) The model neuron, composed of a cell body and neurites with growth cones. (**B**) Symmetry breaking observed in the model neuron (A) with four neurites using Equations (3)–(5). The parameter set of neuron 1 (Supplementary Table IIE) was used. (**C**) Statistical analysis of shootin1 accumulation during neuronal symmetry breaking. The top and bottom panels show the time courses for mean neurite length and mean relative shootin1 concentration in growth cones, respectively. The shootin1 concentration is shown as the multiple of the mean concentration in minor processes (means ± s.e., n=100, 0 min $P<0.001$, −10 min $P<0.001$; compared with minor processes). Red lines indicate the neurite that became an axon, whereas black lines indicate the mean values for the other neurites. (**D**) Impairment of symmetry breaking of the model neuron by continuous active transport of shootin1. Time courses of neurite lengths, each of which develops from randomly selected initial lengths (inset figure). The active transport was computed as 20% of shootin1 at cell body for each time. For good legibility, all lines are arranged at intervals of 1.5 μm (left) and 0.05 (right). Source data is available for this figure at (www.nature.com/msb).

atypical formation of multiple axons in 5% of our model neurons (n=100; Supplementary Figure 4B). Thus, this model reproduces not only typical symmetry-breaking processes involving shootin1 but also atypical behaviors of cultured neurons.

The model neuron simulates a broad range of neuronal behaviors

To validate this model neuron, we finally compared the behaviors of the model with cultured neurons under modified conditions. Elongation of one neurite of stage-2 model neurons by applying mechanical tension led to its axonal specification (Supplementary Figure 4C), as was observed in cultured neurons (Lamoureux *et al*, 2002). Overexpression of shootin1 in the model neuron induced the formation of multiple axons (Supplementary Figure 5A and B), whereas repression of shootin1 inhibited polarization (Supplementary Figure 5D), as observed in cultured neurons (Toriyama *et al*, 2006; Mori *et al*, 2007). In these cases, effects were stronger in the model neuron than in cultured neurons: an eightfold excess level of shootin1 induced the formation of multiple axons in 50% of neurons in the model (Supplementary Figure 5B), whereas a 63-fold excess level (Supplementary Figure 5C) induced multiple axons in 47% of culture neurons (Toriyama *et al*, 2006); a reduction in shootin1 levels to 10% led to the complete inhibition of polarization in the model (Supplementary Figure 5D), whereas an RNAi-mediated reduction in shootin1 levels to 11% (Shimada *et al*, 2008) inhibited the polarization of 52% of neurons at 48 h in culture (Toriyama *et al*, 2006). Treating cultured neurons with cytochalasin D or blebbistatin inhibited the asymmetric accumulation of shootin1 and neuronal polarization (Bradke and Dotti, 1999; Toriyama *et al*, 2006). These drugs inhibit the anterograde

transport of shootin1 (Toriyama *et al*, 2006), and disturb the retrograde flow of actin filaments in the growth cone (Medeiros *et al*, 2006; Shimada *et al*, 2008), which is required to generate traction force for shootin1-induced neurite outgrowth (Shimada *et al*, 2008). The effects of these drugs were also reproduced in the model (Supplementary Figure 5E).

In addition, our model neuron simulated the neurite length-dependent accumulation of shootin1 and axonal regeneration after axonal transection (Figure 8A), which were observed in cultured neurons (Figure 3C–F and Supplementary Figure 6A and B). Interestingly, when axonal transection was performed to leave a short axonal stump, the model neuron showed a stochastic accumulation of shootin1 in multiple growth cones (Figure 8B), as was observed in stage-2 neurons (Figure 1A). In all cases (100%, n=50 neurons), axons regenerated from the neurite that predominantly accumulated shootin1 (arrowheads). We validated this prediction of the model by transecting axons of stage-3 neurons expressing EGFP–shootin1 and mRFP (Figure 8C). As predicted, cultured neurons always exhibited axonal regeneration (100%, n=22 neurons) from the neurite that predominantly accumulated shootin1 (arrowheads). We also compared the distributions of the kinesin-1 motor domain and shootin1 after axonal transection (Supplementary Figure 7, arrows). As in the case of shootin1, Kif5C^{560} accumulated in the regenerating axon. Consistent with the data obtained for stage 2/3 transition (Figure 2),

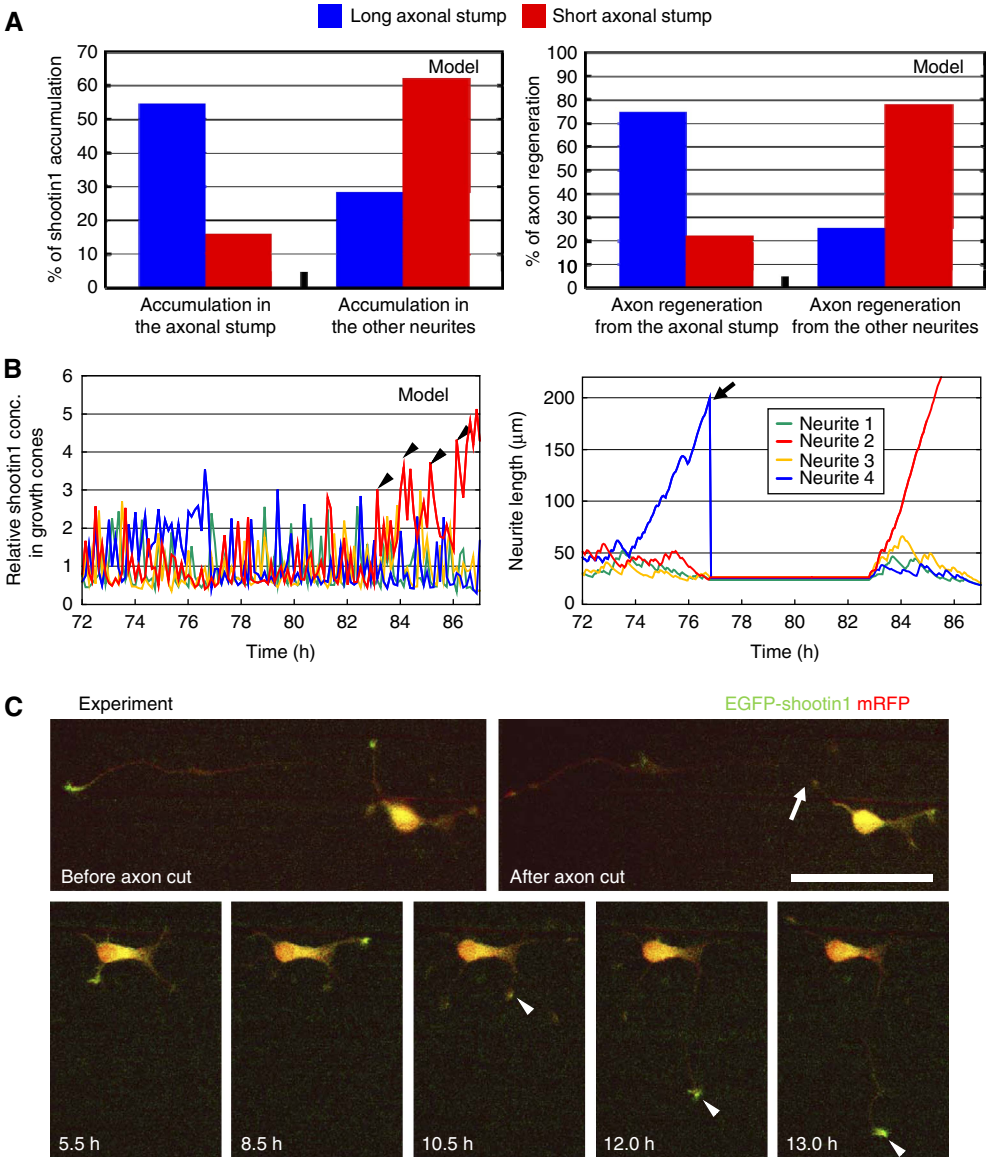

Figure 8 Effects of axonal transection of the model and cultured neurons. (**A**) Shootin1 accumulation and axon regeneration in model neurons after axonal transection. Axonal transections were performed to leave a short or long axonal stump (see Materials and methods section). Data represent the percentages of neurons that accumulated shootin1 in axonal stumps and other neurites (left), and those of neurons that regenerated axons from axonal stumps and other neurites (right). (**B**, **C**) Axonal regeneration from the neurite that predominantly accumulated shootin1. Axonal transections of the model and cultured neurons were performed to leave a short axonal stump (arrows). (B) The neurite length and relative shootin1 concentration in growth cones of a model neuron. (C) A hippocampal neuron expressing EGFP–shootin1 (green) and mRFP (red) was observed under a time-lapse fluorescence microscope. Bar, 50 μm. Source data is available for this figure at (www.nature.com/msb).

Table I Agreements between the behaviors of model and cultured hippocampal neurons

Behaviors	Model data	Experimental data
Under normal conditions		
(1) Stochastic shootin1 accumulation in multiple growth cones before symmetry breaking	Figure 7B	Figure 1A; Ref. (1)[a]
(2) Fluctuation of length of multiple neurites before symmetry breaking	Figure 7B	Figure 1A; Ref. (1, 2)
(3) Shootin1 accumulation before spurt outgrowth of the nascent axon	Figure 7C	Figure 1B
(4) Predominant accumulation of shootin1 in the nascent axon and established axon	Figure 7B and C	Figure 1A and B; Ref. (1)
(5) Polarization of the majority of neurons with different numbers of neurites	Figure 7B and Supplementary Figure S3	Ref. (1, 3)
(6) Replacement of axon-like outgrowth of one neurite by another (atypical behavior)	Supplementary Figure S4A	Ref. (3)
(7) Formation of multiple axons from a minority of neurons (atypical behavior)	Supplementary Figure S4B	Ref. (1, 4, 5)
Under modified conditions		
(8) Axonal specification by applying mechanical tension	Supplementary Figure S4C	Ref. (6)
(9) Formation of multiple axons by shootin1 overexpression	Supplementary Figure S5A and B	Ref. (1, 5)
(10) Inhibition of polarization by decreasing shootin1 level	Supplementary Figure S5D	Ref. (1)
(11) Inhibition of asymmetric accumulation of shootin1 by cytochalasin D or blebbistatin	Supplementary Figure S5E	Ref. (1)
(12) Disturbance of polarization by cytochalasin D or blebbistatin	Supplementary Figure S5E	Ref. (1, 7)
(13) Accumulation of shootin1 in the longest neurite after axonal transaction	Figure 8A	Figure 3C–F
(14) Axonal regeneration from the longest neurite after axonal transaction	Figure 8A	Ref. (2); Supplementary Figure S6B
(15) Axonal regeneration from the neurite that predominantly accumulates shootin1	Figure 8B	Figure 8C

[a]References.
(1) Toriyama *et al* (2006); (2) Goslin and Banker (1989); (3) Dotti *et al* (1988); (4) Jiang *et al* (2005); (5) Mori *et al* (2007); (6) Lamoureux *et al* (2002); (7) Bradke and Dotti (1999).

shootin1 accumulated in the regenerating axon earlier than Kif5C^{560} (arrowheads; n=4). These data further confirm that shootin1 is one of the earliest markers of neuronal symmetry breaking. Overall, the model neuron reproduced a total of 15 neuronal morphological changes and shootin1 dynamics observed under normal and modified conditions (Table I).

Discussion

A novel type of intracellular diffusion system for neurite length sensing

In this study, we demonstrated that shootin1 accumulates in growth cones in a neurite length-dependent manner. Here, the morphological information, neurite length, is translated into a molecular signal, that is, shootin1 concentration in growth cones. We show that the length dependency of shootin1 accumulation is based on its intracellular diffusion (Figure 5E). Although the biological significance of intracellular diffusion is largely unknown, the transcription factor Bicoid is a well-characterized example (Driever and Nusslein-Volhard, 1988; Gregor *et al*, 2007). It forms an anterior–posterior gradient in the syncytium of the *Drosophila* embryo, thereby specifying different regions. The Bicoid gradient is thought to be established by local translation, intracellular diffusion, and subsequent degradation (Gregor *et al*, 2007). In the present system, local protein synthesis and subsequent degradation contribute little, whereas active transport has a critical role. Thus, it represents a distinct type of intracellular diffusion system that translates a morphological property into a molecular signal.

Owing to the simplicity of this mechanism, we consider that the present diffusion system may be extended to include additional molecules. Many diffusible molecules are anterogradely transported in neurites by microtubule-based motor proteins (Hirokawa and Takemura, 2005; Horiguchi *et al*, 2006; Jacobson *et al*, 2006) and by 'wave' structures (Ruthel and Banker, 1998; Zhu *et al*, 2006; Flynn *et al*, 2009). If these molecules have limited expression, turn over slowly, and diffuse back to the cell body, the accumulation of such molecules in growth cones might increase with neurite length as shown here. Furthermore, the spatial dynamics of such molecules might contribute to the early and late steps of neuronal polarization, although this hypothesis requires further analysis.

A core mechanism for neuronal symmetry breaking

The present neurite length-sensing system, together with shootin1-induced neurite outgrowth, constitutes a positive feedback loop (Figure 6A). To analyze the functional role of this feedback loop, we quantitatively modeled length-dependent shootin1 accumulation, shootin1-dependent neurite outgrowth, and shootin1 upregulation. The parameters of these three components were chosen to give the best fit to the quantitative experimental data without any adjustment. The combination of quantitative experimentation and mathematical modeling is regarded as a powerful strategy for attaining a profound understanding of biological systems (Hodgkin and Huxley, 1952b; Lewis, 2008; Meinhardt, 2008; Ferrell, 2009). Without such quantitative modeling based on experimental data, it is difficult to predict the integrated results, even if all

the individual components are known (Hodgkin and Huxley, 1952a; Meinhardt, 2008). In addition, careful comparison between the model predictions and experimental observations would be the only way to test any model: a large number of agreements support the validity of the model. Integrating the three components into a model neuron resulted in spontaneous symmetry breaking. In addition, a model prediction (Figure 8B) was experimentally validated (Figure 8C). Furthermore, there are a total of 15 agreements between the model predictions and the experimental data (Table I). These results suggest that the system described in our model is sufficient to induce neuronal symmetry breaking.

Bolus-like transport of shootin1 by 'waves' caused large stochastic fluctuations in shootin1 concentration in growth cones (Figure 4A). This type of transport seems to be distinct from more gradual delivery through a microtubule-based transport system. Interestingly, the generation of continuous shootin1 transport in our model neuron impaired the symmetry-breaking process (Figure 7D). This is consistent with theoretical models in which feedback amplification of fluctuations in signaling can give rise to robust patterns (Turing, 1952; Meinhardt and Gierer, 2000; Kondo, 2002), and underscores the importance of the stochastic fluctuating signals in spontaneous neuronal symmetry breaking.

Other possible mechanisms and molecules for neuronal symmetry breaking

Recently, Fivaz *et al* (2008) reported a positive feedback interaction between HRas and PI3K in neurite tips, on the basis of which they constructed a mathematical model of neuronal symmetry breaking. Their model, as well as the present one, can be regarded as 'one-takes-all' models, as each growth cone competes for a limited amount of anterogradely transported HRas and shootin1, respectively. However, mechanisms for the competition are distinct between the two models. In the HRas model, the feedback loop between HRas and PI3K enhances HRas transport, for the competitive activation of HRas during symmetry breaking. On the other hand, in the present model, the diffusion-based neurite length-dependent shootin1 accumulation has a key role in the competition (Figure 6A).

As Fivaz *et al* (2008) described, the HRas model involves two assumptions that were not experimentally demonstrated. One is the abovementioned enhancement of HRas transport by the feedback loop. In addition, noise was introduced into the initial conditions of their model for consistent formation of a single axon. Therefore, experimental demonstration of the enhanced transport and noise will be important to confirm that the feedback between HRas and PI3K does mediate a robust symmetry breaking. Our model neuron broke symmetry without enhanced transport, suggesting that the present system represents a minimum mechanism that is sufficient to induce spontaneous neuronal symmetry breaking. Nevertheless, the length-dependent mechanism and polarized transport are compatible with each other. In this regard, Bradke and Dotti (1997) reported that an increased cytoplasmic flow into the future axon precedes axon extension. Thus, it is an interesting possibility that they cooperate to ensure robustness in the symmetry-breaking step.

We reported recently that shootin1 interacts with actin filaments in growth cones (Shimada *et al*, 2008). This interaction may retain shootin1 in growth cones, and thereby have a role in the competitive accumulation. If this interaction is modified in a neurite length-dependent manner or by external signals, the symmetry-breaking step could be further enhanced. We did not incorporate this factor into the present model, for simplicity. This mechanism also remains an issue for future studies.

By focusing on a simple system involving one of the earliest markers of neuronal polarization, shootin1, we could evaluate a core mechanism for neuronal symmetry breaking on the basis of quantitative experimental data. However, it should be noted that agreements between the behaviors of cultured and model neurons are qualitative; there are quantitative differences (also see Supplementary information). For example, shootin1 overexpression and RNAi induced stronger effects in the model neuron than in cultured neurons. This is probably because the model does not involve molecules, such as singar1, which suppress the formation of surplus axons induced by shootin1 overexpression (Mori *et al*, 2007). There are also likely to be additional molecules that cooperate with shootin1 to break neuronal symmetry, as mentioned above. Indeed, a number of molecules are thought to be involved in neuronal polarization (Oliva *et al*, 2006; Arimura and Kaibuchi, 2007; Dajas-Bailador *et al*, 2008; Witte and Bradke, 2008; Barnes and Polleux, 2009). In addition, *in vivo* neuronal polarization is more complicated, involving a number of external factors, including signaling molecules, cell adhesions, and mechanical tensions (Esch *et al*, 2000; Shelly *et al*, 2007). We consider that the present model will provide one of the core mechanisms into which other processes and molecules can be integrated to improve the model's accuracy in future studies.

Materials and methods

Cultures and transfection

Hippocampal neurons prepared from E18 rat embryos were cultured on polylysine- and laminin-coated coverslips as described previously (Mori *et al*, 2007). They were transfected with vectors using Nucleofector (Amaxa) before plating.

DNA constructs

Preparation of the vectors used to express EGFP–shootin1, Kaede–shootin1, and myc–shootin1 has been described earlier (Toriyama *et al*, 2006). mRFP was provided by Dr R. Tsien (University of California, San Diego, CA). The cDNA for kinesin-1 motor domain, $Kif5C^{560}$ (encoding a.a. 1–560 of Kif5C; Jacobson *et al*, 2006), was amplified by PCR from a rat brain cDNA library (Clontech) with primers 5′-GAGAATTCATGGCGGATCCAGCCGAATG-3′ and 5′-GAGA ATTCTATCTCGCCCAGATCCTTGAG-3′, and then subcloned into pEGFP-N2 vector (Clontech). pCAGGS-myc was used to overexpress proteins under the β-actin promoter.

Immunocytochemistry and immunoblot

Immunocytochemistry and immunoblot were performed as described previously (Inagaki *et al*, 2001; Toriyama *et al*, 2006). For CMFDA or CMAC staining, cells were incubated with 5 μM reagent for 2 h before fixation.

Microscopy

Fluorescence and phase-contrast images of fixed neurons were acquired using a fluorescence microscope (Axioplan2; Carl Zeiss) equipped with a charge-coupled device (CCD) camera (AxioCam MRm; Carl Zeiss), and imaging software (Axiovision 3; Carl Zeiss). Time-lapse microscopy was performed at 37°C using a fluorescence microscope (Axio Observer Z1; Carl Zeiss) equipped with a CCD camera (AxioCam MR3; Carl Zeiss), or a fluorescence microscope (IX81N-ZDC; Olympus) equipped with a CCD camera (C4742-80-12AG; Hamamatsu). Fluorescence in the original images was quantified using Multi Gauge software (Fujifilm). Line-scan analysis was performed using MetaMorph software (MDS Analytical Technologies).

Pulse-chase labeling

Day *in vitro* (DIV)-2 hippocampal neurons plated on polylysine- and laminin-coated plastic dishes were starved in methionine/cysteine-free neurobasal medium (Gibco) plus 1 mM glutamine and 0.2% B-27 supplement for 1 h. They were then pulsed for 1 h with 50 μCi/ml [^{35}S]Met/[^{35}S]Cys (EXPRE^{35}S^{35}S Protein Labeling Mix, PerkinElmer), rinsed, and chased with neurobasal medium plus 1 mM glutamine and 0.2% B-27 supplement, together with 2 mM methionine and 2 mM cysteine. The cells were lysed in RIPA buffer (50 mM Tris–HCl (pH 8.0), 1 mM EDTA, 150 mM NaCl, 1% Triton X-100, 0.1% SDS, 0.1% sodium deoxycholate, 2 mM phenylmethylsulfonyl fluoride, and 5 μg/ml leupeptin). Immunoprecipitation was performed with an anti-shootin1 antibody as described previously (Shimada *et al*, 2008). Immunoprecipitated shootin1 was resolved by SDS–PAGE, and the radioactivity associated with shootin1 was visualized by autoradiography and quantified by Multi Gauge.

Axonal transection

The axonal transection experiments in Figure 3C–F were performed to confirm neurite length-dependent shootin1 accumulation. Axons of cultured neurons were mechanically transected using a glass capillary (Sterile Femtotips II, Eppendorf) equipped with a Micromanipulator 5171 (Eppendorf). It has been reported that many hippocampal neurons regenerate axons within 24 h after axonal transection (Goslin and Banker, 1989). We often observed neurons with regenerated axons, even as early as 6 h after transection (Supplementary Figure 6A). Consistent with the previous report (Goslin and Banker, 1989), this axonal regeneration most frequently occurred from the longest neurites (Supplementary Figure 6A and B). In this case, it is difficult to interpret confidently whether the shootin1 accumulation in the regenerated axons is the result of neurite length-dependent shootin1 accumulation or shootin1 accumulation-induced neurite outgrowth, or both. For example, shootin1 may accumulate in the short axonal stump, thereby subsequently inducing neurite outgrowth (Supplementary Figure 6C). Another possibility is that shootin1 may accumulate in the axon regenerated by shootin1 or by some other mechanism (Supplementary Figure 6D). The former case is shootin1 reaccumulation in the short neurite, whereas the latter case is shootin1 reaccumulation in the long neurite. To strictly examine shootin1 reaccumulation by excluding the influence of morphological alteration, we omitted the data for those neurons that regenerated axons. We only analyzed shootin1 reaccumulation in neurons that did not have remarkable morphological changes (Figure 3C, D and F).

We also performed axonal transection of the model neuron. Unlike cultured neurons, the axonal stump of the model neuron retracted rapidly after transection, probably because the model does not have a mechanism to stabilize axonal shafts, for example, by stabilizing axonal microtubules (White *et al*, 1987). Therefore, we held the neurite length of the model constant for 6 h after the transection.

Materials

Preparation of anti-shootin1 antibody has been described previously (Toriyama *et al*, 2006). Antibodies against α-tubulin (DM1A), GFP, and myc were obtained from Sigma-Aldrich, MBL and MBL, respectively. Blebbistatin was obtained from BIOMOL Research Laboratories. CMFDA and CMAC were from Invitrogen.

Statistics and data processing

Statistical significance was determined by the unpaired Student's *t*-test. To reduce noise of the experimental data, the time courses of shootin1 concentration and neurite length were smoothed by $\bar{x}(t) = \frac{1}{5}\sum_{k=-2}^{2} x(t+k)$, whereas those of neurite outgrowth velocity were smoothed by $\bar{v}(t) = \frac{x(t+2)-x(t-2)}{4\Delta t}$.

Modeling of shootin1 diffusion between the growth cone and cell body

If we assume that the shaft is a one-dimensional tube and that shootin1 diffuses passively in the neurite shaft, the rate of shootin1 diffusion from the growth cone to the cell body is proportional to the difference between shootin1 concentrations in the growth cone (C) and the cell body (C_0). When $C-C_0$ is constant, the shootin1 concentration gradient in the neurite shaft is inversely proportional to the neurite length (L), and the retrograde diffusion of shootin1 in the neurite shaft is faster in a shorter neurite than in a longer one (Figure 5E). Thus, the differential equation of shootin1 concentration in the growth cone can be expressed as

$$\frac{dC}{dt} = -\frac{AD}{VL}(C - C_0) \quad (2)$$

where A is the cross-sectional area of the neurite, D the diffusion coefficient, and V the volume of the growth cone. See Supplementary information for detail. Equation (2) follows the well-established Fick's law (van Ooyen *et al*, 2001; Keener, 2002).

Modeling of shootin1-induced neurite outgrowth

We assumed that shootin1-induced neurite outgrowth is regulated primarily by the balance between two mechanical forces, shootin1-induced traction force ($f_s(C)$; Shimada *et al*, 2008) and neurite length-dependent neurite tension ($f_l(L)$; Lamoureux *et al*, 1989), and secondarily by the intracellular concentration (M) of free material molecules required for the construction of the neurite shaft (Figure 6B). As mentioned in Results section, we used tubulin as a representative to approximately describe M in the present analysis. As $f_s(C)$ is dependent on shootin1 concentration (C) in the growth cone and generated by the interaction of shootin1 with other molecules (Shimada *et al*, 2008), we adopted a Hill-type equation to describe it as $f_s(C) \propto \frac{C^h}{K_s^h + C^h}$, where K_s and h are constants. Assuming that $f_l(L)$ is mainly generated by a large strain on the neurite shaft, we introduced a true stress–true strain relationship, used in the field of materials science (Boyer, 1987), to approximate it as the logarithm Hill-type function, $f_l(L) \propto \frac{\ln(L/L_0)}{\ln(K_l/L_0)+\ln(L/L_0)}$, where K_l and L_0 are constants, and $\ln(L/L_0)$ is the true strain (Boyer, 1987) with variable neurite length L. This formula fitted well with the relationship between neurite elongation and neurite tension quantified previously (Lamoureux *et al*, 1989; Supplementary Figure 8).

The velocity of increase in neurite length (L) can be determined as $dL/dt = \delta(k_{on}M - k_{off})$, where δ is the size of the monomer molecule such as tubulin, and k_{on} and k_{off} are the rates of polymerization and depolymerization, respectively (Figure 6B). As cellular cytoskeletal molecules polymerize between a cellular surface and the end of a cytoskeletal filament, the polymerization/depolymerization rates are thought to be affected by tension at the cell surface ($f = f_l(L) - f_s(C)$; Figure 6B; Hill, 1987; Mogilner and Oster, 1996). According to thermodynamic arguments (Hill, 1987), f changes the ratio of the polymerization/depolymerization rates and satisfies the following relationship, $\frac{k_{off}(f)}{k_{on}(f)} = \frac{k_{off}(0)}{k_{on}(0)} \exp\left[\frac{f\delta}{k_B T}\right]$, where k_B is the Boltzmann constant and T is absolute temperature. Therefore, the velocity of elongation and retraction of neurite shaft with cellular tension f can be formulated with the free parameter q as

$$\frac{dL}{dt} = \delta k_{on} \exp[-q\kappa f]M - \delta k_{off} \exp[-(1-q)\kappa f] \quad (6)$$

where $\kappa = \delta/k_B T$. This is called the force–velocity relationship (Hill, 1987). The special case (q=1) of this formula can be derived from the

concept of the ratchet mechanism (Peskin *et al*, 1993; Mogilner and Oster, 1996). As $f=f_l(L)-f_s(C)$ in our model, Equation (6) can be described as

$$\frac{dL}{dt} = \delta k_{on} \exp[pA_s(C) - qA_l(L)]M - \delta k_{off} \exp[-(1-p)A_s(C) + (1-q)A_l(L)] \quad (7)$$

where $A_s(C) = \kappa f_s(C) = \frac{a_s C^h}{K_s^h + C^h}$, $A_l(L) = \kappa f_l(L) = \frac{a_l \ln(L/L_0)}{\ln(K_l/L_0)+\ln(L/L_0)}$, and p is another free parameter.

As the free parameters p and q of Equation (7) may take any value between 0 and 1 inclusive (Hill, 1987; Dogterom and Yurke, 1997), we screened the four representative alternatives of (p,q), (0,0), (1,0), (0,1), and (1,1), to find a suitable formula. Using the experimental data obtained as Figure 6C (n=14 neurites), the set of parameters or their products (a_s, K_s, h, a_l, K_l, L_0, δk_{on}, and δk_{off}) were estimated by fixing M as 15 (we chose 15, as the concentration of free αβ-tubulin dimer in neurons was reported to be about 15 μM (Morris and Lasek, 1984; Mitchison and Kirschner, 1987)), using a least-squares method. Of the four alternatives, the condition of p=q=0 gave the best fit to the experimental data (Supplementary Table III); we therefore chose the equation

$$\frac{dL}{dt} = \delta k_{on} M - \delta k_{off} \exp[-A_s(C) + A_l(L)] \quad (4)$$

to describe the velocity of neurite outgrowth. However, the model neuron successfully polarized in the following analysis, using any of the alternative parameters (p, q)=(0,0), (1,0), (0,1) or (1,1).

Integration of shootin1 upregulation, shootin1-induced neurite outgrowth, and neurite length-dependent shootin1 accumulation in a model neuron

We combined Equations (3)–(5) into a model neuron composed of a cell body and neurites with growth cones (Figure 7A), where C_i is the shootin1 concentration in the i-th growth cone, L_i the length of the i-th neurite, and N the number of neurites. Previous studies reported model neurons with similar variables (Samuels *et al*, 1996; Fivaz *et al*, 2008); for simplicity of the mathematical formulation, our model also does not incorporate the volume of neurite shafts. As the total amount of shootin1 in a neuron S is equal to the sum of the shootin1 levels in the cell body (V_0C_0) and growth cones (VC_i, i=1, …, N), Equation (5) (S) and Equation (3) (dC/dt) can be integrated into the model with the formula $S = V_0C_0 + V\sum_{i=1}^{N} C_i$. As the total concentration of tubulin (T) in a neuron is equal to the sum of free tubulin (M) and the tubulin incorporated in the neurite shafts ($\rho\sum_{i=1}^{N} L_i$), Equation (4) (dL/dt) can be integrated into the model using the formula $T = M + \rho\sum_{i=1}^{N} L_i$, where ρ is a parameter to convert the length of neurite outgrowth (μm) to the consumption of free tubulin concentration for the construction of the elongated neurite shaft. Parameter ρ was estimated from the experimental data obtained in this study and in previous reports (see below). To describe T, we also quantified the α-tubulin expression levels during polarization. The experimental data (blue dots, Figure 6F) were fitted to a Hill-type formula to describe the curve of α-tubulin upregulation (T), $T = \frac{2.9}{1+(t/4480)^{-2.5}} + 1.1$ (blue curve, Figure 6F). All formulae, variables, and parameters used in the model are summarized in Supplementary Table II.

Estimation of the parameter, ρ, which converts the length of neurite outgrowth to the consumption of free tubulin concentration for the construction of the elongated neurite shaft

We used tubulin (Dogterom and Yurke, 1997) to describe M, the concentration of free material molecules for the construction of the neurite shaft, in the present analysis as described in Results section. If we define δ (nm) as the size of a single αβ-tubulin dimer (Figure 6B) and n_t as the average number of protofilaments per single neurite, the number of tubulin dimers necessary for a 1-μm elongation is expressed as $1000n_t/\delta$(molecules). Thus, the cellular concentration of tubulin dimer required to elongate neurite by 1 μm is $1000n_t/V_{tot}\delta$ (molecules/μm^3), where V_{tot} (μm^3) is the total cell volume. As 1 μM is about 600 molecules per μm^3 and δ is 8 nm (Krebs *et al*, 2005), $1000n_t/V_{tot}\delta$ becomes $n_t/4.8V_{tot}$ (μM). As a single microtubule contains 13 protofilaments and a neurite of stage-2 hippocampal neurons contains about 35 (=704/20.5) microtubules (Yu and Baas, 1994), n_t can be estimated as 455. Thus, the tubulin dimer concentration necessary for a 1-μm neurite elongation is expressed as $95/V_{tot}$ μM.

To estimate V_{tot}, we used the data from CMAC staining of cultured hippocampal neurons (Supplementary Figure 1B). As the average radius of neurite shafts was 0.82 μm (n=15), the volume of an L-μm neurite shaft can be approximated as 2 L μm^3. As the line-scan data showed that the average volume of a growth cone (V) was approximately equal to that of a 52-μm neurite shaft (n=9), we estimated V and the average volume of the cell body (V_0) as 104 μm^3 and 1040 μm^3, respectively (note that V_0/V=10, Supplementary Figure 1B). Thus, V_{tot} of neurons with four neurites can be expressed as $1456 + 2L_{tot}$, where L_{tot} is the total neurite length. If we approximate V_{tot} as 2000 μm^3, from this calculation, the concentration necessary for a 1-μm neurite elongation is calculated as 0.048 μM. Previous study reported that the concentration of free αβ-tubulin dimer in neurons was about 15 μM (Morris and Lasek, 1984; Mitchison and Kirschner, 1987), a 310-fold higher concentration for a 1-μm neurite. Thus, in our model, we estimated ρ that converts neurite length L to M, as 1/300.

Supplementary information

Supplementary information is available at the *Molecular Systems Biology* website (www.nature.com/msb).

Acknowledgements

We thank I Smith and Y Bessho for reviewing the paper, and H Sakano, K Minato, T Sugiura, M Nakano and S Noda for discussion. This study was supported in part by MEXT and JSPS KAKENHI, the Global COE Program at NAIST (MEXT), Osaka Medical Research Foundation for Incurable Diseases, and NAIST Interdisciplinary Frontier Research Project.

Conflict of interest

The authors declare that they have no conflict of interest.

References

Arimura N, Kaibuchi K (2005) Key regulators in neuronal polarity. *Neuron* **48:** 881–884

Arimura N, Kaibuchi K (2007) Neuronal polarity: from extracellular signals to intracellular mechanisms. *Nat Rev Neurosci* **8:** 194–205

Barnes AP, Polleux F (2009) Establishment of axon–dendrite polarity in developing neurons. *Annu Rev Neurosci* **32:** 347–381

Boyer HF (1987) *Atlas of Stress Strain Curves*, Ohio: ASM International, Metals Park

Bradke F, Dotti CG (1997) Neuronal polarity: vectorial cytoplasmic flow precedes axon formation. *Neuron* **19:** 1175–1186

Bradke F, Dotti CG (1999) The role of local actin instability in axon formation. *Science* **283:** 1931–1934

Craig AM, Banker G (1994) Neuronal polarity. *Annu Rev Neurosci* **17:** 267–310

Dajas-Bailador F, Jones EV, Whitmarsh AJ (2008) The JIP1 scaffold protein regulates axonal development in cortical neurons. *Curr Biol* **18:** 221–226

Dogterom M, Yurke B (1997) Measurement of the force–velocity relation for growing microtubules. *Science* **278:** 856–860

Dolznig H, Grebien F, Sauer T, Beug H, Mullner EW (2004) Evidence for a size-sensing mechanism in animal cells. *Nat Cell Biol* **6:** 899–905
Dotti CG, Sullivan CA, Banker GA (1988) The establishment of polarity by hippocampal neurons in culture. *J Neurosci* **8:** 1454–1468
Driever W, Nusslein-Volhard C (1988) A gradient of bicoid protein in *Drosophila* embryos. *Cell* **54:** 83–93
Esch T, Lemmon V, Banker G (2000) Differential effects of NgCAM and N-cadherin on the development of axons and dendrites by cultured hippocampal neurons. *J Neurocytol* **29:** 215–223
Ferrell Jr JE (2009) Q&A: systems biology. *J Biol* **8:** 2
Fivaz M, Bandara S, Inoue T, Meyer T (2008) Robust neuronal symmetry breaking by Ras-triggered local positive feedback. *Curr Biol* **18:** 44–50
Flynn KC, Pak CW, Shaw AE, Bradke F, Bamburg JR (2009) Growth cone-like waves transport actin and promote axonogenesis and neurite branching. *Dev Neurobiol* **69:** 761–779
Gauss C, Kalkum M, Lowe M, Lehrach H, Klose J (1999) Analysis of the mouse proteome. (I) Brain proteins: separation by two-dimensional electrophoresis and identification by mass spectrometry and genetic variation. *Electrophoresis* **20:** 575–600
Goslin K, Banker G (1989) Experimental observations on the development of polarity by hippocampal neurons in culture. *J Cell Biol* **108:** 1507–1516
Gregor T, Wieschaus EF, McGregor AP, Bialek W, Tank DW (2007) Stability and nuclear dynamics of the bicoid morphogen gradient. *Cell* **130:** 141–152
Hill TL (1987) *Linear Aggregation Theory in Cell Biology*. New York: Springer-Verlag
Hirokawa N, Takemura R (2005) Molecular motors and mechanisms of directional transport in neurons. *Nat Rev Neurosci* **6:** 201–214
Hodgkin AL, Huxley AF (1952a) The dual effect of membrane potential on sodium conductance in the giant axon of Loligo. *J Physiol* **116:** 497–506
Hodgkin AL, Huxley AF (1952b) A quantitative description of membrane current and its application to conduction and excitation in nerve. *J Physiol* **117:** 500–544
Horiguchi K, Hanada T, Fukui Y, Chishti AH (2006) Transport of PIP3 by GAKIN, a kinesin-3 family protein, regulates neuronal cell polarity. *J Cell Biol* **174:** 425–436
Inagaki N, Chihara K, Arimura N, Menager C, Kawano Y, Matsuo N, Nishimura T, Amano M, Kaibuchi K (2001) CRMP-2 induces axons in cultured hippocampal neurons. *Nat Neurosci* **4:** 781–782
Jacobson C, Schnapp B, Banker GA (2006) A change in the selective translocation of the kinesin-1 motor domain marks the initial specification of the axon. *Neuron* **49:** 797–804
Jiang H, Guo W, Liang X, Rao Y (2005) Both the establishment and the maintenance of neuronal polarity require active mechanisms: critical roles of GSK-3beta and its upstream regulators. *Cell* **120:** 123–135
Jiang H, Rao Y (2005) Axon formation: fate versus growth. *Nat Neurosci* **8:** 544–546
Keener JP (2002) *Computational Cell Biology*. New York: Springer-Verlag, pp 171–197
Kondo S (2002) The reaction–diffusion system: a mechanism for autonomous pattern formation in the animal skin. *Genes Cells* **7:** 535–541
Krebs A, Goldie KN, Hoenger A (2005) Structural rearrangements in tubulin following microtubule formation. *EMBO Rep* **6:** 227–232
Lamoureux P, Buxbaum RE, Heidemann SR (1989) Direct evidence that growth cones pull. *Nature* **340:** 159–162
Lamoureux P, Ruthel G, Buxbaum RE, Heidemann SR (2002) Mechanical tension can specify axonal fate in hippocampal neurons. *J Cell Biol* **159:** 499–508
Lewis J (2008) From signals to patterns: space, time, and mathematics in developmental biology. *Science* **322:** 399–403
Marshall WF (2004) Cellular length control systems. *Annu Rev Cell Dev Biol* **20:** 677–693
Medeiros NA, Burnette DT, Forscher P (2006) Myosin II functions in actin-bundle turnover in neuronal growth cones. *Nat Cell Biol* **8:** 215–226
Meinhardt H (2008) Hans Meinhardt. *Curr Biol* **18:** R401–R402
Meinhardt H, Gierer A (2000) Pattern formation by local self-activation and lateral inhibition. *Bioessays* **22:** 753–760
Mitchison TJ, Kirschner MW (1987) Some thoughts on the partitioning of tubulin between monomer and polymer under conditions of dynamic instability. *Cell Biophys* **11:** 35–55
Mogilner A, Oster G (1996) Cell motility driven by actin polymerization. *Biophys J* **71:** 3030–3045
Mori T, Wada T, Suzuki T, Kubota Y, Inagaki N (2007) Singar1, a novel RUN domain-containing protein, suppresses formation of surplus axons for neuronal polarity. *J Biol Chem* **282:** 19884–19893
Morris JR, Lasek RJ (1984) Monomer-polymer equilibria in the axon: direct measurement of tubulin and actin as polymer and monomer in axoplasm. *J Cell Biol* **98:** 2064–2076
Neumann FR, Nurse P (2007) Nuclear size control in fission yeast. *J Cell Biol* **179:** 593–600
Oliva Jr AA, Atkins CM, Copenagle L, Banker GA (2006) Activated c-Jun N-terminal kinase is required for axon formation. *J Neurosci* **26:** 9462–9470
Peskin CS, Odell GM, Oster GF (1993) Cellular motions and thermal fluctuations: the Brownian ratchet. *Biophys J* **65:** 316–324
Ruthel G, Banker G (1998) Actin-dependent anterograde movement of growth-cone-like structures along growing hippocampal axons: a novel form of axonal transport? *Cell Motil Cytoskeleton* **40:** 160–173
Ruthel G, Banker G (1999) Role of moving growth cone-like 'wave' structures in the outgrowth of cultured hippocampal axons and dendrites. *J Neurobiol* **39:** 97–106
Samuels DC, Hentschel HG, Fine A (1996) The origin of neuronal polarization: a model of axon formation. *Philos Trans R Soc London B Biol Sci* **351:** 1147–1156
Shelly M, Cancedda L, Heilshorn S, Sumbre G, Poo MM (2007) LKB1/STRAD promotes axon initiation during neuronal polarization. *Cell* **129:** 565–577
Shimada T, Toriyama M, Uemura K, Kamiguchi H, Sugiura T, Watanabe N, Inagaki N (2008) Shootin1 interacts with actin retrograde flow and L1-CAM to promote axon outgrowth. *J Cell Biol* **181:** 817–829
Toriyama M, Shimada T, Kim KB, Mitsuba M, Nomura E, Katsuta K, Sakumura Y, Roepstorff P, Inagaki N (2006) Shootin1: a protein involved in the organization of an asymmetric signal for neuronal polarization. *J Cell Biol* **175:** 147–157
Turing A (1952) The chemical basis of morphogenesis. *Philos Trans R Soc London B Biol Sci* **237:** 37–72
Van de Water III L, Olmsted JB (1980) The quantitation of tubulin in neuroblastoma cells by radioimmunoassay. *J Biol Chem* **255:** 10744–10751
van Ooyen A, Graham BP, Ramakers GJA (2001) Competition for tubulin between growing neurites during development. *Neurocomputing* **38:** 73–78
White LA, Baas PW, Heidemann SR (1987) Microtubule stability in severed axons. *J Neurocytol* **16:** 775–784
Witte H, Bradke F (2008) The role of the cytoskeleton during neuronal polarization. *Curr Opin Neurobiol* **18:** 479–487
Yu W, Baas PW (1994) Changes in microtubule number and length during axon differentiation. *J Neurosci* **14:** 2818–2829
Zhu PP, Soderblom C, Tao-Cheng JH, Stadler J, Blackstone C (2006) SPG3A protein atlastin-1 is enriched in growth cones and promotes axon elongation during neuronal development. *Hum Mol Genet* **15:** 1343–1353